inventions

MDPI

Article

The Separation of Microalgae Using Dean Flow in a Spiral Microfluidic Device

Ming-Lung Lee [1] and Da-Jeng Yao [1,2,*]

[1] Institute of NanoEngineering and MicroSystems, National Tsing Hua University, Hsinchu 30013, Taiwan; minglee@micron.com

[2] Department of Power Mechanical Engineering, National Tsing Hua University, Hsinchu 30013, Taiwan

* Correspondence: djyao@mx.nthu.edu.tw

Received: 15 May 2018; Accepted: 18 June 2018; Published: 21 June 2018

Abstract: A cell-in-droplet encapsulation using Dean flow in a spiral microfluidic device was applied to separate microalgae. In recent years, researchers have been interested in separating micro particles using microfluidic chips because of its great advantages in relation to various applications such as in biotechnology, medical examination, and cell studies. The main disadvantage of these microfluidic chips is particle clogging that decreases the separation yield, which then creates difficulties during the investigation of the particles. The microfluidic chip that is introduced in this work is a combination of two distinct designs—a spiral microchannel design to separate microalgae of various sizes, and a microdroplet generation design for cell encapsulation. The yield of the separation is enhanced through the concept of dominant forces (Dean drag force and lift force) in a spiral microchannel design, together with a design of the microdroplet generation that narrows the volume to facilitate cell observation. We report the development of cells, particle separation, and microdroplet generation. Using the spiral microchannel design can solve the clogging problem by distributing the microalgae evenly for the microdroplet generation section. A spiral microfluidics design was used as a separator for the different sized particles and a microdroplets generation design was used to encapsulate the separated particles. As for the design for the microdroplets generation section, a 3-way microchannel was designed. In this research, two kinds of microalgae have been used: the smaller one is chlorella vulgaris and the bigger one is cosmarium. Because of all of these benefits, this device might be an alternative for cell applications using droplet-based platforms. With a different channel height design, the separation efficiency for Chlorella vulgaris is about 75–80% and for Cosmarium is about 60–72%.

Keywords: microalgae separation; spiral microfluidic device; microdroplet; dean flow

1. Introduction

The separation of microparticles and filtration based on size are essential for many applications in diverse fields, including medical examinations, environmental or biochemical applications, or even cell studies [1]. Consequently, the advantages of using microspheres in applications such as drug delivery, bone tissue engineering and regeneration, absorption and desorption of substances, and likes kinetic release of the loaded drug components are also presented [2]. Moreover, different methods for the separation of cells or particles have been developed, removing the microparticles from solutions such as membrane filter [3]. However, micropillars or pore filtrations have a high probability of particle clogging because of the exact pore size of the filter [4]. As cells become lodged in the microscale constrictions during the separating process, the overall hydrodynamic resistance of the filter changes and diminishes the effect of the applied pressure gradient [4]. Because of this clogging problem, several membrane-less separation techniques have been introduced, for example sedimentation [5], field-flow fractionation [6], hydrodynamic chromatography [7], pinched-flow fractionation [8], electrophoresis [9,

10], dielectrophoresis [11], acoustic separation [12], diffusion-based extraction [13,14], deterministic lateral displacement [15–17], centrifugation [18–20], and inertial focusing [21,22]. Even though these membrane-less techniques make clogging less likely to occur, some disadvantages remain. For example, electrophoresis and dielectrophoresis provide a high resolution of particle separation, however they both require an external power source and generate heat that might harm the cells over a long operating period [23,24]. The use of curved microchannels can avoid the disadvantages of previous microfluidic chip designs that might require external applied forces or complicated system integration.

In this work, we introduce a simple approach for the continuous passive separation of microparticles in microchannels using size-dependent inertial migration, i.e., centrifugally based. In 1961, Segre and Silberberg first demonstrated the principle of inertial migration in a circular tube on a macroscale. The experiment was conducted to make particles migrate and form a narrow band near the channel walls [25]. For the inertial migration of particles in microchannels, a circular tube was subsequently altered to have a square or rectangular cross section to obtain a maximum separation [1,23,26–29].

In recent years, researchers have become interested in micro particles because of their promising applications in various related fields [1]. The study of microparticles is essential for many applications in diverse biological fields. Many traditional methods for the separation of cells or particles, and also for the removal of microparticles from solutions, involve the use of a membrane filter such as micropillars or pore filtrations of other types which have a high probability of particle clogging because of the exact pore size of the filter. Because of this clogging problem, several membrane-less separation techniques have subsequently been introduced—for example, sedimentation and dielectrophoresis [11].

2. Method

2.1. Theory

Fluid flow through a curvilinear channel is subject to various parameters, such as centrifugal acceleration that is directed radially outward, leading to the formation of two counter-rotating vortices, known as Dean vortices, in the top and bottom halves of the channel [1]. The magnitude of these secondary flows is quantified with a dimensionless Dean number (D_e) given by:

$$D_e = \frac{\rho U_f D_h}{u}\sqrt{\frac{D_h}{2R}} = Re\sqrt{\frac{D_h}{2R}} \quad (1)$$

In which ρ denotes the density of the fluid medium (kg/m^3), U_f is the average fluid velocity (m/s), μ is the fluid viscosity (kg m^{-1} s^{-1}), R is the radius of the curvature (m) of the path of the microchannel, and Re is the flow Reynolds number. For a straight microchannel, $D_e = 0$, indicating the absence of Dean flows. In a curved channel, D_e increases with increasing curvature (smaller R), increasing channel size (larger D_h), and more rapid flow (larger Re). Dean flows increase in magnitude with increasing D_e and have been used to demonstrate efficient fluid mixing in microchannels [26,29]. D_h stands for the hydraulic diameter of which the formula is:

$$D_h = \frac{2ab}{2(a+b)} \quad (2)$$

In this equation, a denotes the width and b denotes the height of the microchannel.

Depending on the particle size, a drag force (F_D) causes particles to move with the Dean vortices, and thus move towards either the inner or the outer microchannel wall. In addition to this drag force, particles in a curvilinear channel experience forces from pressure and inertial lift [28]. The net lift force (F_L) acts on the particles that tend to occupy equilibrium positions for which the oppositely directed lift forces are equal, and also forms narrow bands. Particles experience both forces near the outer microchannel wall, where net lift force F_L acts along the direction of F_D and the particles continue to follow the Dean vortices, independent of their size. However, near the inner microchannel wall,

F_L and F_D act in opposite directions and depending on the magnitude of these forces, the particles will balance and form a focused stream or continue to re-circulate the Dean vortex [1,27]. Illustrations of this phenomenon is demonstrated in Figure 1.

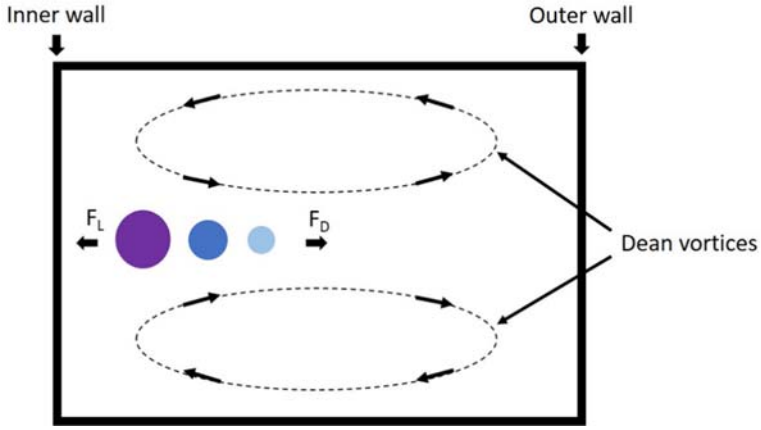

Figure 1. The schematic cross section of a curved microchannel, illustrating the focusing positions of particles of varied size. The lift force and the Dean drag force are highlighted. (Redrawn from ref [28]).

$$F_D = 5.4 \times 10^{-4} \pi \mu De^{1.63} a_p \quad (3)$$

$$F_L = \rho G^2 C_L {a_p}^4 \quad (4)$$

Another parameter that must be considered is ratio $\frac{a_p}{\nu}$ of the particle confinement, where a_p denotes the particle diameter and ν is the smallest channel dimension. This ratio $\frac{a_p}{\nu}$ must be ≥ 0.07 for particles to be focused [1,21,28].

2.2. Design of the Microfluidic Device

Because every parameter would affect the Dean number-particle size, the dimension of the microchannel, flow rate, Dean drag force and lift force—and this would definitely affect the separation of mixed particles—several parameters must be fixed to obtain an accurate result. In this spiral microfluidic design section, the fixed parameters are specified in Table 1.

Table 1. Fixed parameters for calculations.

Particle Size	Radius of Curvature (*R*)	Flow Rate
5 μm 50 μm	1.5 mm	10 μL h^{-1}

Particle sizes 5 μm and 50 μm are used here because the average size of Chlorella vulgaris is approximately 5 μm and the average size of Cosmarium is 50 μm. The initial curve or the radius of curvature is fixed at 1.5 mm, whereas the flow rate of the medium is fixed at 10 μL h^{-1}.

Other than those fixed parameters, there are some numbers that are invariant throughout the calculation. These are mostly physical properties of water as water serves as the medium and those that are applied to the fluids participating in the microchannel shown in Table 2.

Table 2. Constant used for equations.

Density	Dynamic Viscosity	Lift Coefficient (C_L)
1000 kg/m^3	10^{-3} kg m^{-1} s^{-1}	0.5

Lift coefficient C_L is a function of the particle position across the channel cross section, for which we assume an average value of 0.5 [1,21]. After the fixed parameters and constants are defined, the objective is to vary the dimensions of the spiral microchannel to observe the most suitable Dean numbers (D_e), Dean drag force (F_D), lift force (F_L), and the length required for the Dean migration (L_D). The widths of the channels are 100 µm and 200 µm, with heights ranging from 70 µm through to 130 µm and 180 µm.

Table 3 lists the calculated Dean numbers for the varied dimension of the microchannel, 70 µm through to 130 µm and 180 µm. The larger the Dean number, the greater the Dean drag force, which hence makes the particles equilibrate more rapidly [29]. The next step is to take the Dean number to calculate the Dean drag and lift forces for particles of size 5 µm and 50 µm. Table 4 lists the results; orange columns are the outcomes for 5 µm particles and the green columns are for the 50 µm particles.

Table 3. The relationship between the dimension of the microchannel and the Dean number.

Dimension (HxW)		Dean Number, D_e
70 µm	100 µm	0.005414489
	200 µm	0.003825606
130 µm	100 µm	0.004688801
	200 µm	0.003858315
180 µm	100 µm	0.004107533
	200 µm	0.003674157

Table 4. Comparison between Dean drag force and lift force for 5 µm and 50 µm particles.

Dimension (HxW)		Drag Force, F_{D5} (N)	Drag Force, F_{D50} (N)	Lift Force, F_{L5} (N)	Lift Force, F_{L50} (N)
70 µm	100 µm	1.7148×10^{-15}	1.7148×10^{-14}	2.90236×10^{-17}	2.90236×10^{-15}
	200 µm	9.73453×10^{-16}	9.73453×10^{-15}	4.57573×10^{-18}	4.57573×10^{-14}
130 µm	100 µm	1.35626×10^{-15}	1.35626×10^{-14}	4.46609×10^{-18}	4.46609×10^{-14}
	200 µm	9.87056×10^{-16}	9.87056×10^{-15}	5.74618×10^{-19}	5.74618×10^{-15}
180 µm	100 µm	1.09308×10^{-15}	1.09308×10^{-14}	1.80082×10^{-18}	1.80082×10^{-14}
	200 µm	9.11424×10^{-16}	9.11424×10^{-15}	2.07301×10^{-19}	2.07301×10^{-15}

Two results of the calculations are that the values are small and that some numbers are close together, even though the dimensions of the microchannels differ. The reason for this is that the flow rate is set as 10 µL h^{-1} for each channel size. Another aspect that can explain why the lift force tends to have a larger value for a smaller cross-sectional area in the expression for the lift force is that there is a factor called shear rate of the fluid (G) [29], which is

$$G = \frac{U_{max}}{D_h} \quad (5)$$

where U_{max} is the maximum flow velocity and D_h is the dean number of particles. In Equation (2), the hydraulic diameter is determined directly from the size of the microchannel, which explains why the lift force decreases as the cross-sectional area of the microchannel increases.

According to research on particle or cell separation which used methods including designs of spiral microfluidics and microdroplet generation, each design has its own advantages and disadvantages. For this new microfluidic chip design, we optimized the device by combining two designs into one and having a spiral microfluidic design to separate particles of varied size and using the microdroplet generation design to encapsulate the separated particles. The hope is that this design enhances the separation efficiency together with possible further applications after the particle encapsulation. The original idea was inspired by a review of the literature of work from

Kemna's group [29], where they also used droplet-based microfluidic systems to create cell droplet encapsulations using a curved continuous microchannel. The underlying concept is the use of the Dean-couple inertial in the microchannel, so that particles pass through the microdroplet generation junction to make particle encapsulation. The design concept is shown in Figure 2. The sorting microalgae will be encapsulated by the oil inlet and the medium inlet, using Y-shaped structures. To combine a spiral sorting design and a droplet generation formation, the whole system will be shown in Figure 3. Once the microalgae were separated by the spiral structure, the microalgae would be encapsulated in the microdroplets with microdroplet generation.

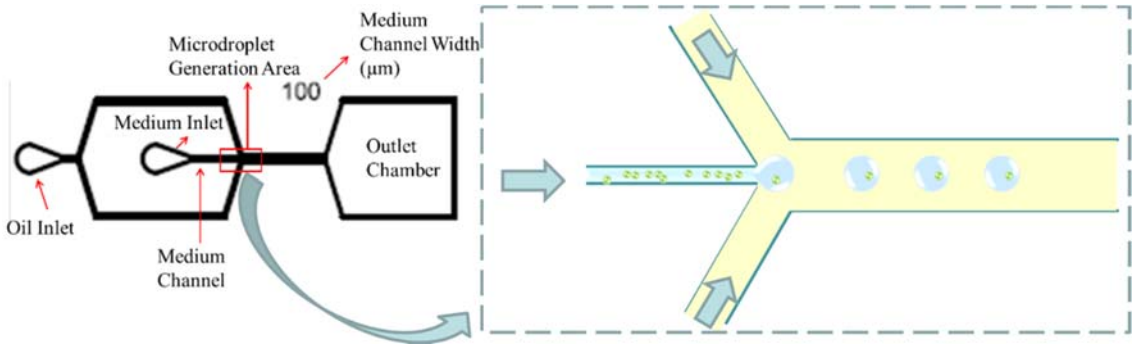

Figure 2. The design concept of microdroplet generation.

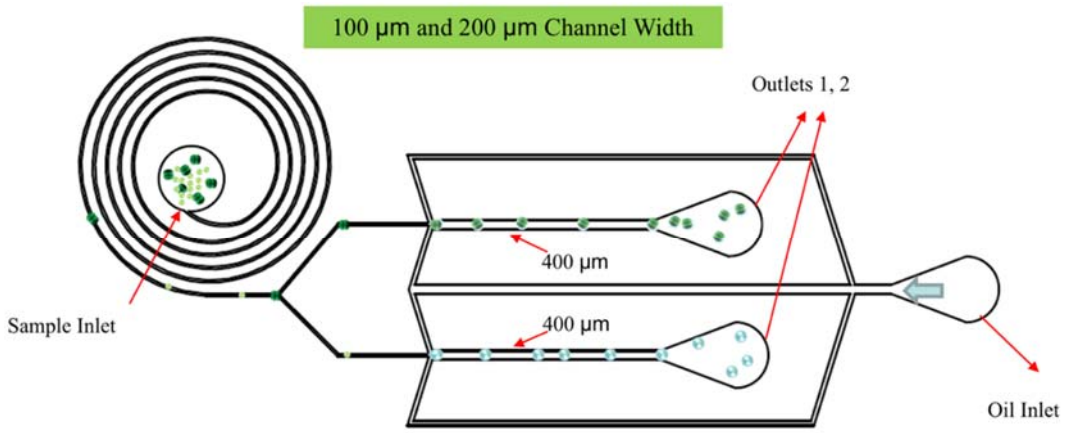

Figure 3. The whole microfluidic chip.

Several factors were developed from the first microfluidic design, including the microchannel height and the position for each part inside the microfluidic chip. The combined microfluidic chip concept design can be finalized as in Figure 3.

2.3. Device Fabrication

This microfluidic device was fabricated using soft lithography to create a microchannel according to the designs. In the field of micro design, soft lithography has been widely used to produce structural patterned surfaces and coatings with specific biomolecules. The process can be divided into two main parts—making the microfluidic mold and making the microchannel from polydimethylsiloxane (PDMS), before finally bonding the polymer to a glass slide.

Figure 4 shows the complete process of making a microfluidic device using soft lithography, from creating a mold from a blank to bonding the PDMS to a glass slide, according to the mold fabrication steps. The detailed process has the following steps:

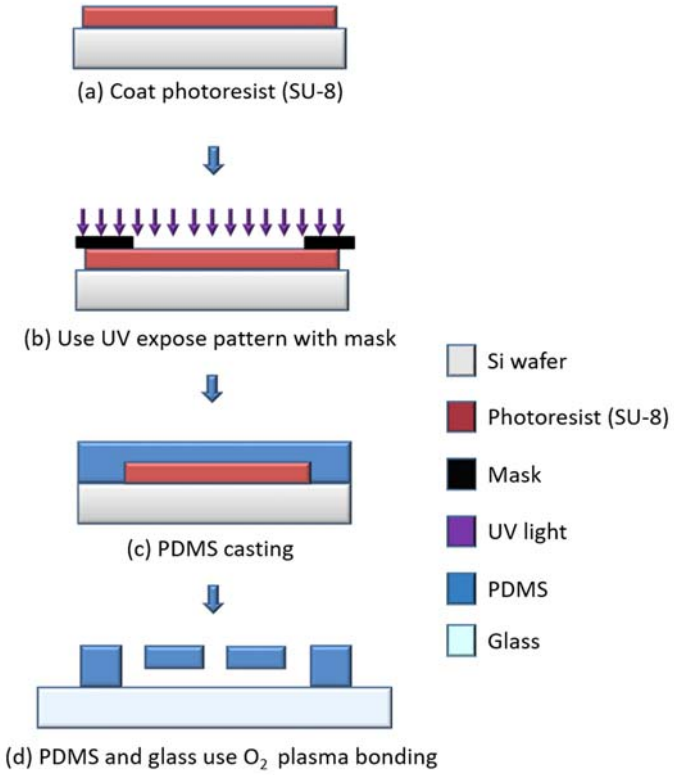

Figure 4. A schematic diagram of the microfluidic device fabrication process.

The cleaning can be done with acetone, isopropanol (IPA), and deionized water to rinse the surface of the wafer accordingly. Having a clean standard eliminates possible particles that might affect the quality of the mold. Nitrogen is used to blow away the liquid on the wafer surface, and then the wafer is baked on a hotplate at 120 °C until it is completely dry. After the standard cleaning, the next step involves piranha cleaning (a solution of sulfuric acid and hydrogen peroxide in ratio 7:1). The use of this solution requires its heating to 90 °C. After this temperature is reached, the wafer is immersed in the piranha solution for 10 min, before rinsing again with deionized water. The main purpose of piranha cleaning is to ensure that organic residues and particles are also very effectively removed, which the standard cleaning cannot do. The wafer is baked again on a hot plate until it is completely dry. The photoresist (PR) in this experiment is SU-8 3050. This type of PR coating is a negative photoresist process such that any area exposed to ultraviolet light (UV) becomes hard, whereas the blocked area would all disappear during the development. When the coating of the wafer with PR is complete, the wafer is baked on a hot plate at 65 °C, and the temperature is increased by 5 °C every 3 min until 95 °C is reached, at which baking is continued for another 15 min. After the wafer cools to 23 °C, it is ready for the UV exposure which is intended to create a pattern on the wafer. The wafer is taken to the UV exposure machine stage and is aligned along three axes (X, Y, Z). The alignment of every wafer is important because it might affect the UV light distribution and patterning. The UV intensity must be measured every time before an exposure because the number indicates the duration of the exposure. A single-sided UV exposure machine is used to undertake the photolithography according to a calculated duration. Baking is required after the UV exposure to ensure that the PR coating will remain in place, and to harden the PR coating. The procedure is similar to the soft baking. The last step in the fabrication of the mold is the development of the pattern on the wafer. The wafer is soaked in SU-8 developer solution. The PR coat that is not exposed to ultraviolet light dissolves in the solution. This step must be carefully implemented, and the pattern must be closely examined. If the PR coat is over-developed, the pattern turns out poorly. After the development, the wafer is rinsed with deionized water and baked until it is dry. After all of the device

fabrication steps, the final mold can be achieved as in Figure 5. The design includes varied sizes of the medium microchannel, and the numbers inside the design indicate the size for the medium channel. Otherwise, they all have the same dimension.

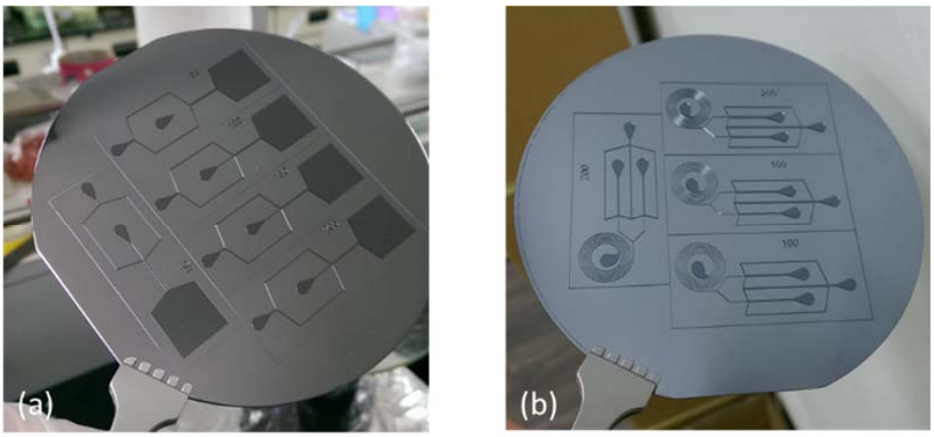

Figure 5. The finished molds for a microfluidic device: (**a**) Design from Figure 2; (**b**) Design from Figure 3.

Microchannels are generally fabricated through the direct micro-machining of silicon or glass. Microfabrication over glass or silicon is typically expensive, tedious, and labor-intensive. For microfabricated devices to ease their way into the scientific community, the cost, ease of fabrication, and functionality must be addressed. A transparent, viscoelastic organic polymer (polydimethyl siloxane) can serve as an alternative for micro-fabrication to the costlier and time-consuming methods for glass and silicon. PDMS is considered as a widely used polymer in the fabrication of microfluidic chips because of its unique properties, such as transparency, biocompatibility, and its low cost of fabrication, relative to other methods. The PDMS used in this research (Dow Corning® SYLGARD 184 silicone elastomer) arrives as solutions A and B, where solution A is the silicone base, and solution B is the curing agent. The mixture ratio for PDMS (A:B) is 10:1. The detailed steps of the PDMS fabrication follow.

The PDMS solutions, both A and B, are weighed. The ratio for solution A to solution B is 10:1: solution A (20 g) and solution B (2 g). After thorough mixing, the mixed PDMS is poured on the pattern mold, as shown in Figure 4c, before being baked at 85 °C for 20 min. This baking hardens the fluid PDMS. The inlet and outlet of the microfluidic channel will be drilled first. After that, the PDMS bonds on the glass slide, using oxygen plasma. In order to avoid PDMS completely, bonds to the glass slide causes the inlet and outlet to block. After that, the microfluidic chip bonding is followed by oxygen plasma.

Our technique for microfluidic chip bonding is the use of an oxygen plasma. Such a surface treatment is a popular technique for bonding two materials together, which in this case is PDMS and a glass slide. The oxygen plasma imposes a modification of the surface in order to enhance its bonding strength. O_2 plasma has been used to clean and modify the surface of PDMS and the glass to become clean and hydrophilic to improve its bonding strength. Once the surfaces of the two materials are in contact, they react by bonding, where the PDMS bonds to the glass slide to create tight microchannels. The PDMS with its pattern is placed upwards, together with a glass slide and is rinsed with IPA to clean the surfaces. After the surfaces are clean, the oxygen-plasma generator is used to scan through the surfaces of both materials (PDMS and the glass slide), and they then bond together, as in Figure 4d. The final chip is baked on a hot plate at 65 °C for roughly 15 min to ensure that the PMDS is bonded tightly with the glass slide. Subsequently, small tubes are fixed with both inlets and outlets (with AB adhesive glue) to act as connectors from the tube to the chip in the experiment. After this process is completed, the microfluidic chip is ready for operation.

2.4. Cosmarium and Chlorella Vulgaris Are Used in the Experiments

Cosmarium, a genus of algae belonging to the Desmidiaceae family, is used in many and diverse applications, for example, as an indicator of the sensitivity of photosynthesis to UV radiation [30], and to observe species-specific differences both at optimal and stress temperatures [31,32]. The size of microalgae of this kind ranges from 20 µm to 80 µm. Cosmarium has a unique structure that can be directly identified as it has a circular shape with a ring right in the middle; Figure 6b shows an image of Cosmarium. Chlorella vulgaris is a genus of single-cell green algae belonging to phylum Chlorophyta. Its shape is spherical, its diameter varies from 2 µm to 10 µm, and it lacks flagella, as in Figure 6a. Chlorella vulgaris contains the green photosynthetic pigments. Through photosynthesis, it multiplies rapidly, requiring only carbon dioxide, water, sunlight, and minerals in small amounts to reproduce. Chlorella vulgaris is commonly believed to serve as a potential source of food and energy because its photosynthetic efficiency can theoretically attain 8% [33]. Not only might Chlorella vulgaris be a great food source because it contains 45% protein, 20% fat, 20% carbohydrate, 5% fiber, and ten minerals and vitamins, algae of this type are also predicted to be an alternative medicine to treat cancer [34]. Methods of mass production are currently being applied to cultivate it in large artificial circular ponds. In the 1960s, scientists mentioned that it is impossible for human beings and other animals to digest Chlorella vulgaris in its natural state because of the tough cell walls encapsulating the nutrients [34]. Research on Chlorella vulgaris has continued, and its possibility as a new food source has been debated.

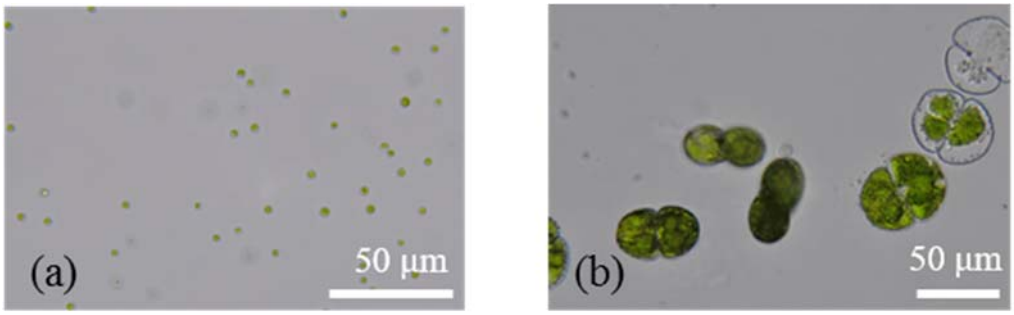

Figure 6. (**a**) Chlorella vulgaris has a spherical-shape, its diameter varies from 2 µm to 10 µm, and it lacks flagella; (**b**) Cosmarium has a circular-shape with a ring right in the middle. The scale bar is 50 µm.

2.5. Experiments

After several designs, both for the microdroplet generation and various microchannel widths and heights, together with spiral designs also with varied widths and heights of the microchannels, the final dimensions for the combined designs were separated into two main groups according to channel widths. The first group had widths of 100 µm, and the second group had widths of 200 µm for a spiral channel of heights 70, 130, and 180 µm. Also, for the setup of the experiment, the fixed parameters included flow rate 10 µL h^{-1} of the medium, flow rate 80 µL h^{-1} of the oil phase using a syringe pump (KDS210), and the duration of the experiment was about 1 h. Table 5 is a summary of the fixed parameters of every experiment made for the microfluidic chips of the combined design.

Table 5. Summary of fixed parameters for each channel dimension.

Channel Width	Channel Height	Oil Flow Rate	Medium Flow Rate
100 µm 200 µm	70 µm 130 µm 180 µm	80 µL h^{-1}	10 µL h^{-1}

3. Results and Discussion

3.1. ANSYS Simulations

For the new design of the microfluidic channels, ANSYS simulations were undertaken to ensure that the pairs of flow rates from oil and the medium are suitable for microdroplet generation. Such a simulation can provide a prediction of the microdroplet generation according to the change of color of the fluids inside the channels. Our laboratory has ANSYS simulation software (ANSYS 15.0, ANSYS, Inc., Pittsburgh, PA, U.S.A.). To run the simulations, the models must first be created in a three-dimensional structure using an existing design and turned into a three-dimensional mode with AutoCAD software (AutoCAD 2015, Autodesk Inc., San Rafael, CA, USA). From that source, the AutoCAD file is imported to the ANSYS software simulation for the meshing (point calculations on the model's surface), and the file is again imported into Fluent to run the fluid simulations. Fluent simulation is sub-software running for ANSYS 15.0, showing the simulation in an animated film. Several settings must be inputted into the software to obtain the most precise result in the Fluent simulation. For the setup, the properties of the solutions and the microfluidic chip were required.

For the spiral channel for the particle separation, the simulation software was used with the addition of particles inside the fluid. To simulate the particle separation, particles of two sizes must be input. Because of the wide range of the size of Chlorella vulgaris and Cosmarium, an average size of each for the simulation was selected to be 5 µm and 50 µm. To add the particles to flow in the same channel in the same Fluent interphase in the model's tab, the discrete phase should be on. From that, the particle sizes are set up. For the first spiral design, the width of the channel was set to 100 µm and 200 µm (100 µm in Figure 7). The flow rate for the medium was 10 µL h^{-1}, and the sizes of the particles were 5 µm and 50 µm. In Figure 7, the red dots represent 50 µm particles of Cosmarium, and blue dots represent 5 µm particles of Chlorella vulgaris. According to the Equations (3) and (4), the smaller particles would remain at the outer wall of the microchannel and the larger particles would stick at the inner wall. This concept is visible in this simulation for the blue dots, however the red dots were all stuck inside the inner spiral loops.

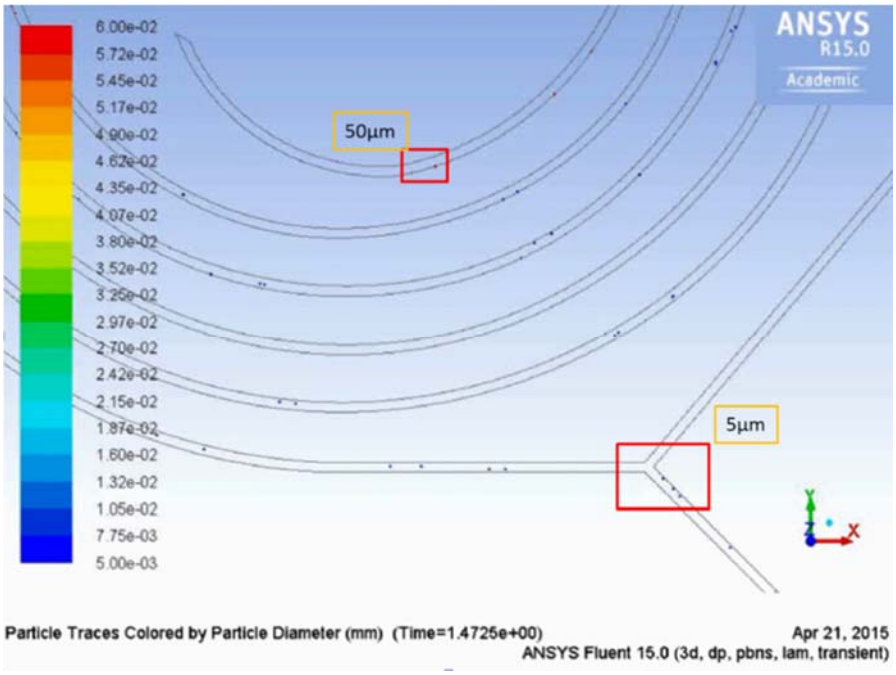

Figure 7. The simulation photo, where the red dots represent 50 µm particles and the blue dots represent 5 µm particles.

To improve the microdroplet generation of the microfluidic channels design, ANSYS software was utilized to simulate the flow rate. Afterwards, the velocity of the oil phase was 80 μL h^{-1} and the medium phase was 10 μL h^{-1} and 20 μL h^{-1}. The results of different medium flow rates are shown in Figure 8. The best pair of the flow rate is when the oil has a flow rate of 80 μL h^{-1} and the medium is 10 μL h^{-1}, as shown in Figure 8a. Even though the one with the oil has a flow rate of 80 μL h^{-1} and the medium is 20 μL h^{-1}, as shown in Figure 8b, this shows a similar size and result to those shown in Figure 8a. The medium of 20 μL h^{-1} had a speed that was a lot faster than the one with 10μL h^{-1}, which would make it hard for the microdroplet observation, and therefore might not suitable for this experiment. A comparison was observed for the microdroplets under different flow rates (medium phase was 10 μL h^{-1} and 20 μL h^{-1}). Due to the simulation, the medium phase (10 μL h^{-1}) was used in our experiment.

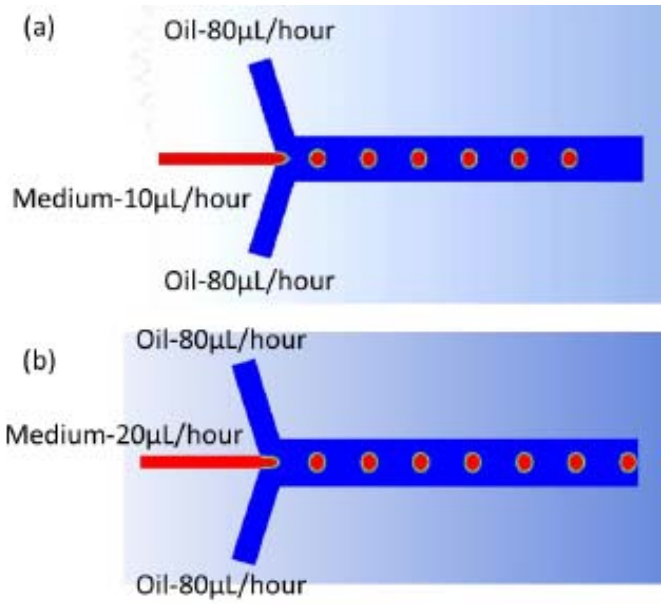

Figure 8. The schematic that was obtained from ANSYS simulation. (**a**) The oil flow rate is 80 μL/hour and the medium is 10 μL h^{-1}; (**b**) The oil flow rate is 80 μL/hour and medium is 20 μL h^{-1}.

3.2. The Combination Microfluidic Chip Design

3.2.1. Design with a Spiral Channel Width of 100 μm

The data were generated by counting the number of microalgae of each type at the separation junction. The upper separation junction led to the first section for microdroplet generation, whereas the lower separation junction channel led to the second section for microdroplet generation. According to the equations and calculations, the smaller particles should be favored toward the outer microchannel wall, while the larger particles tend to stick to the inner microchannel wall. From the graph, the fraction was calculated at the separation junction and was converted into a percentage, which represents the wanted particles flowing into that particular microchannel. In this research, microalgae of two kinds were used: the smaller was Chlorella vulgaris and the larger was Cosmarium. The color represented in the graph is yellow for Chlorella vulgaris and purple for Cosmarium. According to the theory, Chlorella vulgaris would prefer to flow into the upper channel that is connected from the outer spiral channel, and Cosmarium would move into the lower channel that is connected from the inner spiral

channel. The separation efficiency was calculated according to the number of wanted microalgae divided by the total number of microalgae from the two channels; the simple equation is [29]

$$E_i = \frac{N_i}{N_{ti}} \times 100\% \quad (6)$$

In which E_i denotes the separation efficiency of the microalgae of interest, N_i is the number of microalgae in the particular channel, and N_{ti} is the total number of microalgae of interest from both channels. In Figure 9, with the same width (100 µm) of the spiral channel, there is no significant difference for the Chlorella vulgaris separation for each channel height, and the percentage ranged from about 77 to 82%. In contrast, there was an obvious result of different heights for Cosmarium. The one of height 70 µm had the greatest separation efficiency of 72.5%, whereas channel heights 130 and 180 µm had an efficiency of about 62–63% for Cosmarium. These results are also linked to the earlier calculations, which shows that the larger the channel height is, the better the separation for Cosmarium. However, there is no significant effect for Chlorella vulgaris.

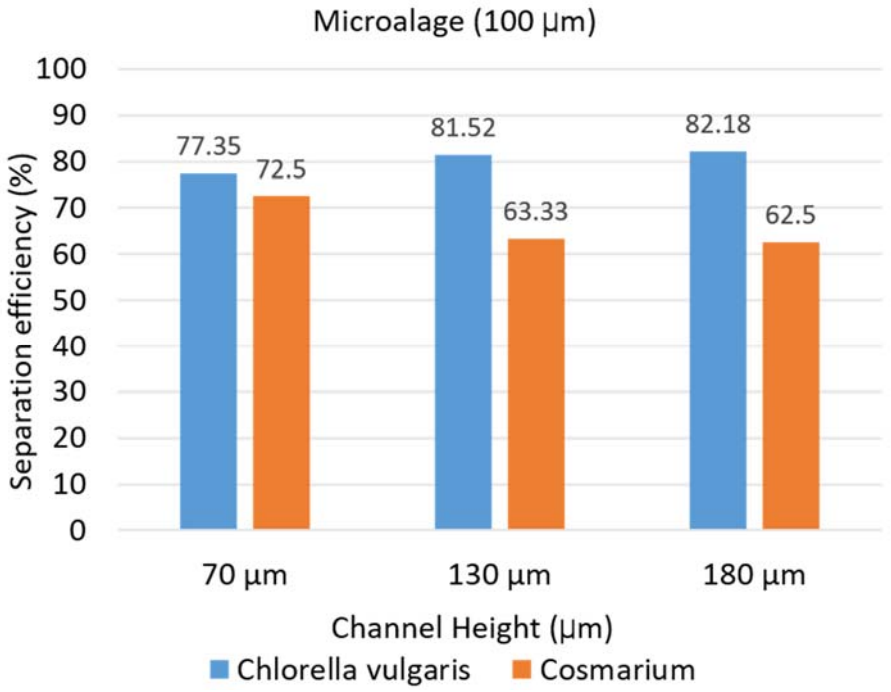

Figure 9. Separation efficiency of microalgae in a spiral channel of width 100 µm, between the three channel heights—70, 130, and 180 µm.

3.2.2. Design with a Spiral Channel Width of 200 µm

The concepts of the separation efficiency and the design of the spiral channel of width 200 µm are the same as for width 100 µm. Figure 10 shows the average separation efficiency for each of the heights, 70, 130, and 180 µm. The overall result for this 200 µm group can be discussed as, within the same channel width (200 µm), there is no significant difference of separation efficiency for Cosmarium. Cosmarium is represented as purple bars, having a value of 60–63% for all heights, however the number was more noticeable for Chlorella vulgaris. The yellow bars stand for the Chlorella vulgaris, having a separation efficiency of about 75 to 80%. Also, the bigger channel heights have a greater separation efficiency compared to the 70 µm channel height. This outcome was also related to the equation as predicted earlier. The heights for the 200 µm microchannel width do not affect Cosmarium much, in contrast to Chlorella vulgaris.

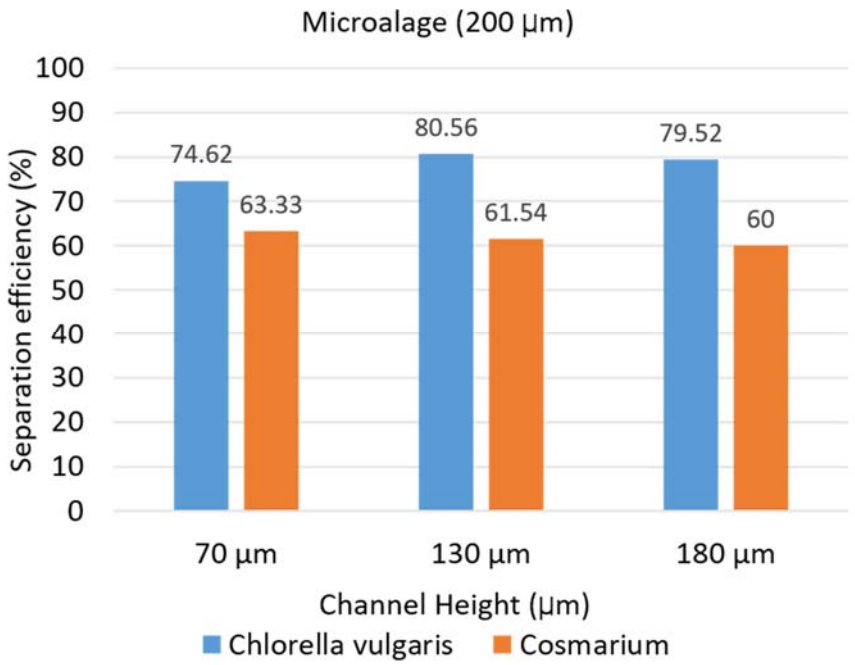

Figure 10. The separation efficiency of microalgae in a spiral channel of width 200 μm, between three channel heights—70, 130, and 180 μm.

4. Conclusions

The aim of this work was to undertake the self-size-based separation of particles in a mixture of sizes using a Dean flow. A spiral microchannel in the first section made the particles separate according to their sizes, followed by microdroplet generation to encapsulate the microalgae.

A spiral microchannel design can solve the problem of clogging to distribute the microalgae evenly for the microdroplet generation section. If the particles are more uniform, the encapsulation efficiency increases. The spiral microchannel with all related forces in the channel would help to sort the particles through their variation of size. The larger particles would experience a greater lift force, making them stay near the inner wall of the microchannel, whereas the smaller particles would experience more of the Dean drag force, resulting in them staying nearer the outer wall. By means of this principle, particles of varied size can be separated with no external setup or pretreatment of samples.

Author Contributions: M.-L.L. conducted the simulation, chip fabrication, experimental measurement and analysis under the guidance of D.-J.Y.

Funding: The funding was from Ministry of Science and Technology under grants MOST 104-2221-E-007-078-MY2.

Acknowledgments: The authors would like to thank Fan-Gang Tseng for the chip fabrication facilities from the Department of Engineering and System Science at National Tsing Hua University, Hsinchu, Taiwan. Yi-Ju Liu from food industry research and development institute, Hsinchu 30062, Taiwan, for the help of microalgae preparation and providing fabrication facilities.

Conflicts of Interest: The authors declare no conflict of interest.

References

1. Bhagat, A.A.S.; Kuntaegowdanahalli, S.S.; Papautsky, I. Continuous particle separation in spiral microchannels using dean flows and differential migration. *Lab Chip* **2008**, *8*, 1906–1914. [CrossRef] [PubMed]
2. Hossain, K.M.Z.; Patel, U.; Ahmed, I. Development of microspheres for biomedical applications: A review. *Prog. Biomater.* **2015**, *4*, 1–19. [CrossRef] [PubMed]

3. Yoon, Y.; Kim, S.; Lee, J.; Choi, J.; Kim, R.K.; Lee, S.J.; Sul, O.; Lee, S.B. Clogging-free microfluidics for continuous size-based separation of microparticles. *Sci. Rep.* **2016**, *6*, 26531. [CrossRef] [PubMed]
4. McFaul, S.M. Physical Cell Separation Using Microfluidic Funnel Ratchets. Ph.D. Thesis, University of British Columbia, Vancouver, BC, Canada, 2011.
5. Shin, S.; Shardt, O.; Warren, P.B.; Stone, H.A. Membraneless water filtration using CO_2. *Nat. Commun.* **2017**, *8*, 15181. [CrossRef] [PubMed]
6. Giddings, J. Field-flow fractionation: Analysis of macromolecular, colloidal, and particulate materials. *Science* **1993**, *260*, 1456–1465. [CrossRef] [PubMed]
7. Chmela, E.; Tijssen, R.; Blom, M.T.; Gardeniers, H.J.G.E.; van den Berg, A. A Chip System for Size Separation of Macromolecules and Particles by Hydrodynamic Chromatography. *Anal. Chem.* **2002**, *74*, 3470. [CrossRef] [PubMed]
8. Yamada, M.; Nakashima, M.; Seki, M. Pinched Flow Fractionation: Continuous Size Separation of Particles Utilizing a Laminar Flow Profile in a Pinched Microchannel. *Anal. Chem.* **2004**, *76*, 5465–5471. [CrossRef] [PubMed]
9. Xu, X.; Caswell, K.K.; Tucker, E.; Kabisatpathy, S.; Brodhacker, K.L; Scrivens, W.A. Size and shape separation of gold nanoparticles with preparative gel electrophoresis. *J. Chromatogr. A* **2007**, *1167*, 35–41. [CrossRef] [PubMed]
10. Lin, H.-C.; Liu, Y.-J.; Yao, D.-J. Core—Shell droplets for parallel DNA ligation of an ultra-micro volume using an EWOD microfluidic system. *JALA J. Assoc. Lab. Autom.* **2010**, *15*, 210–215. [CrossRef]
11. Dürr, M.; Kentsch, J.; Müller, T.; Schnelle, T.; Stelzle, M. Microdevices for manipulation and accumulation of micro- and nanoparticles by dielectrophoresis. *Electrophoresis* **2003**, *24*, 722–731. (In English) [CrossRef] [PubMed]
12. Nilsson, A.; Petersson, F.; Jonsson, H.; Laurell, T. Acoustic control of suspended particles in micro fluidic chips. *Lab Chip* **2004**, *4*, 131–135. [CrossRef] [PubMed]
13. Brody, J.P.; Yager, P. Diffusion-based extraction in a microfabricated device. *Sens. Actuators A Phys.* **1997**, *58*, 13–18. [CrossRef]
14. Jandik, P.; Weigl, B.H.; Kessler, N.; Cheng, J.; Morris, C.J.; Schulte, T.; Avdalovic, N. Initial study of using a laminar fluid diffusion interface for sample preparation in high-performance liquid chromatography. *J. Chromatogr. A* **2002**, *954*, 33–40. [CrossRef]
15. Huang, L.R.; Cox, E.C.; Austin, R.H.; Sturm, J.C. Continuous Particle Separation Through Deterministic Lateral Displacement. *Science* **2004**, *304*, 987. [CrossRef] [PubMed]
16. Inglis, D.W.; Davis, J.A.; Austin, R.H.; Sturm, J.C. Critical particle size for fractionation by deterministic lateral displacement. *Lab Chip* **2006**, *6*, 655–658. [CrossRef] [PubMed]
17. Beech, J.P.; Tegenfeldt, J.O. Tuneable separation in elastomeric microfluidics devices. *Lab Chip* **2008**, *8*, 657–659. [CrossRef] [PubMed]
18. Gregoratto, I.; McNeil, C.J.; Reeks, M.W. Micro-devices for rapid continuous separation of suspensions for use in micro-total-analysis-systems (μTAS). *Proc. SPIE* **2007**, *6465*. [CrossRef]
19. Seo, J.; Lean, M.H.; Kole, A. Membraneless microseparation by asymmetry in curvilinear laminar flows. *J. Chromatogr. A* **2007**, *1162*, 126–131. [CrossRef] [PubMed]
20. Seo, J.; Lean, M.H.; Kole, A. Membrane-free microfiltration by asymmetric inertial migration. *Appl. Phys. Lett.* **2007**, *91*, 033901. [CrossRef]
21. Di Carlo, D.; Irimia, D.; Tompkins, R.G.; Toner, M. Continuous inertial focusing, ordering, and separation of particles in microchannels. *Proc. Nat. Acad. Sci. USA* **2007**, *104*, 18892–18897. [CrossRef] [PubMed]
22. Di Carlo, D.; Edd, J.F.; Irimia, D.; Tompkins, R.G.; Toner, M. Equilibrium Separation and Filtration of Particles Using Differential Inertial Focusing. *Anal. Chem.* **2008**, *80*, 2204–2211. [CrossRef] [PubMed]
23. Kuntaegowdanahalli, S.S.; Bhagat, A.A.S.; Kumar, G.; Papautsky, I. Inertial microfluidics for continuous particle separation in spiral microchannels. *Lab Chip* **2009**, *9*, 2973–2980. [CrossRef] [PubMed]
24. Hsu, C.-T.; Yao, D.-J.; Ye, K.-J.; Yu, B. Renewable energy of waste heat recovery system for automobiles. *J. Renew. Sustain. Energy* **2010**, *2*, 013105. [CrossRef]
25. Segré, G.; Silberberg, A. Behaviour of macroscopic rigid spheres in Poiseuille flow Part 2. Experimental results and interpretation. *J. Fluid Mech.* **1962**, *14*, 136–157. [CrossRef]
26. Bhagat, A.; Kuntaegowdanahalli, S.; Papautsky, I. Inertial microfluidics for continuous particle filtration and extraction. *Microfluid. Nanofluid.* **2009**, *7*, 217–226. (In English) [CrossRef]

27. Bhagat, A.A.S.; Kuntaegowdanahalli, S.S.; Papautsky, I. Enhanced particle filtration in straight microchannels using shear-modulated inertial migration. *Phys. Fluids (1994-present)* **2008**, *20*, 101702. [CrossRef]
28. Hasni, A.E.; Göbbels, K.; Thiebes, A.L.; Bräunig, P.; Mokwa, W.; Schnakenberg, U. Focusing and Sorting of Particles in Spiral Microfluidic Channels. *Procedia Eng.* **2011**, *25*, 1197–1200. [CrossRef]
29. Kemna, E.W.M.; Schoeman, R.M.; Wolbers, F.; Vermes, I.; Weitz, D.A; van den Berg, A. High-yield cell ordering and deterministic cell-in-droplet encapsulation using Dean flow in a curved microchannel. *Lab Chip* **2012**, *12*, 2881–2887. [CrossRef] [PubMed]
30. Marija, S.; Dieter, H. Sensitivity of photosynthesis to UV radiation in several Cosmarium strains (Zygnematophyceae, Streptophyta) is related to their geographical distribution. *Photochem. Photobiol. Sci.* **2014**, *13*, 1066–1081. [CrossRef] [PubMed]
31. Stamenković, M.; Woelken, E.; Hanelt, D. Ultrastructure of Cosmarium strains (Zygnematophyceae, Streptophyta) collected from various geographic locations shows species-specific differences both at optimal and stress temperatures. *Protoplasma* **2014**, *251*, 1491–1509. [CrossRef] [PubMed]
32. Neale, P. Species-Specific Responses to Combined Thermal-irradiance Stress in Microalgae—Each is to its Own. *Photochem. Photobiol.* **2013**, *89*, 822–823. [CrossRef] [PubMed]
33. Zelitch, I. 9-Relation of Photosynthesis, Total Respiration, and other Factors to Control of Productivity in Stands. In *Photosynthesis, Photorespiration, and Plant. Productivity*; Academic Press: Cambridge, MA, USA, 1971; pp. 267–299.
34. Belasco, W. Algae Burgers for a Hungry World? The Rise and Fall of Chlorella Cuisine. *Technol. Cult.* **1997**, *38*, 608–634. [CrossRef]